Pd_2Ga nanorods as highly active bifunctional catalysts for electrosynthesis of acetic acid coupled with hydrogen production

Qiuxia Wang[a], Junfeng Liu[a,*], Tong Li[a], Ting Zhang[b], Jordi Arbiol[b,c], Suxia Yan[a], Yong Wang[a], Huaming Li[a], Andreu Cabot[c,d,*]

a Institute for Energy Research, School of Chemistry and Chemical Engineering, Jiangsu University, Zhenjiang, 212013, China

b Catalan Institute of Nanoscience and Nanotechnology (ICN2), CSIC and BIST, Campus UAB, Bellaterra, 08193, Barcelona, Spain

c ICREA, Pg. Lluis Companys 23, 08010, Barcelona, Spain

d Catalonia Institute for Energy Research (IREC), Sant Adrià de Besòs, 08930 Barcelona, Spain

** Corresponding authors*

E-mail: jliu@ujs.edu.cn (J. Liu), acabot@irec.cat (A. Cabot)

Abstract: The production of hydrogen from water splitting is hampered by the sluggish oxygen evolution reaction (OER). To overcome the OER limitation, herein we propose the electrosynthesis of value-added acetic acid from ethanol as the anodic reaction. For this strategy to be cost-effective, we develop a bifunctional catalyst based on Pd_2Ga nanorods. Such Pd_2Ga/C-based catalyst presents a high activity, selectivity and also stability for the electrocatalytic ethanol-to-acetic acid conversion with a current density above 164 mA cm^{-2} and a mass activity of 1.97 A mg^{-1}_{Pd}. Besides, its activity for hydrogen production is comparable to that of Pt/C catalysts. Using Pd_2Ga/C as a bifunctional catalyst for both water reduction at the cathode and ethanol oxidation at the anode, these two coupled reactions are demonstrated to be an energy-efficient approach for the simultaneous production of high purity acetic acid and hydrogen. The assembled electrolyzer requires a small voltage input of 0.62 V to reach a current density of 10 mA cm^{-2}, much lower than that of cells based on commercial Pt/C or Pd/C catalyst. The high performance of the coupled system relies on a combination of an electronic and

bifunctional effect of Ga, reducing the hydrogen-binding energy on the Pd site and at the same time actively participating in the reaction by providing OH^- binding sites.

Keywords: Palladium gallium; coupled system; ethanol oxidation reaction; hydrogen production; electrocatalysis

1. Introduction

Hydrogen is a clean energy carrier with a high energy density. The electrocatalytic water splitting, involving the anodic oxygen evolution reaction (OER) and the cathodic hydrogen evolution reaction (HER), has been extensively studied as a promising sustainable technology to produce high-purity hydrogen fuels.[1-6] However, the sluggish four-electron transfer OER, the related high overpotentials required (>1.6-1.7 V versus RHE), and the use of expensive catalysts with moderate stabilities strongly limit this technology.[7-9]

A promising strategy to reduce energy consumption is to replace the sluggish OER with the electrooxidation of an organic species.[10-15] Among the possible organic substrates, ethanol possesses unique properties of low toxicity, high boiling point for safe storage, transportation and operation, and potential sourcing from biomass fermentation.[16] Owing to these advantages, the electrocatalytic ethanol oxidation reaction (EOR) has attracted much attention for its application in direct alcohol fuel cells.[17,18] However, fewer studies have concentrated on the coupling of EOR with HER to replace OER in the water-splitting process.[11,19] This coupled system can avoid the risk of explosion of hydrogen and oxygen mixing. More importantly, the electrocatalytic EOR is a thermodynamically favorable process that requires much lower overpotentials and provides a high energy conversion efficiency compared with OER.[7] In addition, the oxidation of ethanol can be used

to produce various fine chemicals.[11,20-22] As an example, the electrooxidation of ethanol in the 4-electron C2 pathway can produce acetic acid, which is a value-added product. This ethanol-to-acetic acid conversion is actually considered an appealing energy-efficient pathway for the synthesis of acetic acid in moderate conditions and with high selectivity.[22] Therefore, the coupling of the acetic acid synthesis at the anode with the hydrogen production at the cathode is highly attractive both from energetic and economic points of view. Thus, the development of highly active, stable and selective catalysts for both EOR to acetic acid and HER is a worthwhile endeavor.

Non-precious metal-based catalysts have been extensively studied as efficient HER catalysts but they show poor EOR activity.[23-27] Pt and Pd are highly active catalysts for both HER and EOR, but suffer from poisoning by the reaction intermediates, especially in the EOR process.[28-33] Compared with Pt, Pd is a relatively more abundant metal, and provides better resistance to poisoning, thus it has attracted increasing attention in recent years.[16] However, the activity and stability Pd needs to be further improved to meet the commercial demands. An effective strategy to improve the catalytic performance, both in terms of activity and stability, is the alloying of Pd with additional metals.[34-36] Particularly, the alloying with a less electronegative element can promote electron transfer to Pd active sites. Such negatively charged Pd is considered favorable to the desorption of reaction intermediates, thus improving the EOR and HER activity and stability.[37]

Herein, Ga, with a much lower electronegativity (1.81) than Pd (2.20) is selected as the alloying element to produce intermetallic Pd_2Ga.[38] Taking advantage of colloidal synthesis methods, monodisperse Pd_2Ga particles with well-defined morphology can be produced. Such Pd_2Ga are mixed with carbon and tested as a bifunctional catalyst for both EOR and HER. The measured excellent HER activity and the outstanding EOR catalytic performance, well above that of Pd/C and Pt/C, motivated

us to test this catalyst in a two-electrode electrolyzer, using it for both anode and cathode. The assembled device delivers a high current density at much lower cell voltages than those required in a cell-based on commercial Pd/C and Pt/C catalysts. More importantly, this system exhibits excellent selectivity, being able to produce high purity acetic acid in the anode while producing hydrogen at the cathode.

2. Experimental section

2.1. Chemicals and Materials

Palladium(II) acetylacetonate ($Pd(acac)_2$, Pd 34.9%), Gallium acetylacetonate ($Ga(acac)_3$, 99%), oleylamine (OAm, approximate C18 content 80-90%), acetic acid (99.8%), methylamine hydrochloride (MAC, 98%), Nafion (10 wt % in water) and deuterium oxide (D_2O, 99.9%) were purchase from Macklin. Commercial Pd/C (10% Pd) catalyst was obtained from Bide Pharmatech Ltd. Platinum on carbon (Pt 20%) was purchased from Alfa Aesar. Potassium hydroxide, chloroform and ethanol were of analytical grade and purchased from Sinopharm Chemical Reagent Co. Ltd. (Shanghai, China). All reagents were used as received without further purification.

2.2. Synthesis of Pd_2Ga nanorods

In a typical synthesis, 60.9 mg (0.2 mmol) of $Pd(acac)_2$, 73.4 mg (0.2 mmol) of $Ga(acac)_3$, 67.5 mg (1 mmol) of MAC and 10 mL of OAm were added into a 25 mL three-neck flask equipped with a condenser. The system was heated to 100 °C in 8 min under nitrogen flow and maintained at this temperature for 30 min to remove low boiling point impurities, moisture and oxygen. Then the temperature was increased to 220 °C in 10 min and kept there for 1 h before cooling down to ambient temperature. The black product was isolated by adding an excess amount of ethanol and centrifuging

at 5000 rpm for 3 min. Purification was achieved by multiple dispersion/precipitation steps using chloroform and ethanol. Finally, the powder was suspended in 5 mL of chloroform in a vial.

2.3. Characterization

X-ray diffraction (XRD) was collected from the sample supported on a silica glass substrate on a Bruker-AXS D8 X-ray diffractometer with Cu Kα radiation (λ = 1.5418 Å) operating at 40 kV and 40 mA. Transmission electron microscopy (TEM) characterization was carried out using a ZEISS LIBRA 120, operating at 120 kV and a JEOL 1011 operating at 100 kV. Carbon-coated TEM grids from Ted-Pella were used as substrates. High-resolution TEM (HRTEM) studies were conducted using a field emission gun FEI™ Tecnai F20 microscope at 200 kV with a point-to-point resolution of 0.19 nm. High angel annular dark-field scanning transmission electron microscope (HAADF-STEM) was combined with electron energy loss spectroscopy (EELS) in the Tecnai F20, by using a GATAN QUANTUM filter. Scanning electron microscopy (SEM) analyses were done in a ZEISS Auriga microscope with an energy-dispersive X-ray spectroscopy (EDS) detector operating at 20 kV. X-ray photoelectron spectroscopy (XPS) was analyzed on a Thermo Scientific K-Alpha XPS system equipped with an Al Kα source (hv= 1486.6eV) operating at 12 kV and 6 mA, and binding energy values were referred to the adventitious C 1s peak at 284.8 eV.

2.4. Preparation of catalysts

5 mg of carbon black was added to the vial containing of as-synthesized nanomaterials with 5 mL of chloroform. The mixture was sonicated for 2 h to support the Pd_2Ga nanorods on the carbon, then Pd_2Ga/C was collected by centrifugation. To remove residual ligands from the surface of the nanorods, Pd_2Ga/C was redispersed in a mixture of 8 mL of ethanol and 1mL of acetic acid, followed by

sonication for another 2 h. Afterwards, multiple washing steps were carried out using ethanol and chloroform separately, and dried naturally under ambient conditions. 5 mg of the final product was dispersed in 1 mL of deionized water/ethanol (v/v = 1: 1) and 20 μL of 5% Nafion solution, and sonicated for 2 h to form a homogeneous catalyst ink. For comparison, catalysts ink of commercial Pd/C and commercial Pt/C were prepared by sonicating 5 mg of Pd/C or Pt/C with the same amount of Nafion, deionized water and ethanol mixture.

2.5. Electrochemical measurements

Electrochemical measurements were conducted on a CHI660E electrochemical workstation (CH Instruments Inc., Shanghai) at room temperature using a standard three-electrode system. A platinum mesh was used as the counter electrode and a Hg/HgO (1 M KOH) electrode was used as the reference electrode. The working electrode was prepared by drop-casting 3.0 μL of the catalyst ink on a glassy carbon electrode (GCE, 3 mm in diameter) and posterior drying naturally at room temperature. The precise amount of Pd loaded on the GCE determined by inductively coupled plasma optical emission spectrometry (ICP-OES), was 5.9 μg of Pd for Pd_2Ga/C catalyst. For EOR measurement, the cyclic voltammetry (CV) curves were recorded from -1.0 to 0.4 V versus Hg/HgO at a scan rate of 50 mV s^{-1} in N_2-saturated aqueous solutions that contained 0.5 M KOH or 0.5 M KOH + 0.5 M ethanol. The linear sweep voltammetry (LSV) tests were conducted at a scan rate of 10 mV s^{-1}. Chronoamperometry (CA) measurements were conducted at -0.1 V versus Hg/HgO in a 0.5 M KOH + 0.5 M ethanol electrolyte. For HER measurements, polarization curves were tested from -0.9 V to -1.5 V versus Hg/HgO in 0.5 M KOH + 0.5 M ethanol solution. The Faradaic efficiency (FE) was measured by the volumetric method, comparing the actual volume of hydrogen evolution with the theoretical one.

2.6. Computational details

All calculations were carried out using the Vienna Ab initio Simulation Package (VASP) code [39,40]. The Perdew-Burke-Ernzerhof [41] functional with a generalized gradient approximation [42] was adopted to describe the electronic exchange-correlation energy. The projector augmented-wave [43] was applied and the energy cutoff was 400 eV. The sampling over Brillouin zone was treated by the Monkhorst-Pack type and k-point mesh with a 3×3×1 grid was introduced. The long-range van der Waals (vdW) interactions were described by using the DFT-D3 method with Becke-Johnson damping [44,45]. Geometry optimization was considered to be converged until the maximal residual energy and force were less than 10^{-5} eV and -0.03 eV/Å, respectively. A vacuum slab of 15 Å was applied in z-direction to avoid the pseudo interactions between the periodic units. The Pd (111) and Pd_2Ga (211) surfaces with four atomic layers were chosen to construct the investigated periodic slab models. During optimization, the top two layers were relaxed and the bottom two layers were fixed. Thermodynamic free energies were defined as $G= E_{DFT} + E_{ZPE} - TS$, Where E_{DFT}, E_{ZPE}, and TS denote the DFT total energy, zero-point energy (ZPE), and entropy, respectively.

3. Results and discussion

Pd_2Ga particles were produced by a novel colloidal synthesis method, using $Pd(acac)_2$ and $Ga(acac)_3$ as metal precursors, OAm as the solvent, and Cl^- released from MAC as a selective ligand directing the particle geometry (see the experimental section for details).[46,47] Fig. 1a displays a representative TEM micrograph of the particles obtained using the above-detailed procedure. They displayed elongated morphologies with an average length of 20 nm and width of 7 nm (Fig. 1c). As shown in Fig. 1b, the XRD pattern of such nanorods (NRs) displayed an orthorhombic phase with

Pnma space group, matching the reference pattern from Pd_2Ga (JCPDS 03-065-1511). No additional diffraction peaks corresponding to secondary phases were observed. HRTEM analysis confirmed the Pd_2Ga orthorhombic phase with lattice parameters a = 5.4762 Å, b = 4.0570 Å and c = 7.7973 Å (Fig. 1d-f). STEM-EELS elemental composition maps demonstrated the presence of Pd and Ga, being both elements homogeneously distributed within each NR and throughout all the NRs (Fig. 1g). SEM-EDS analysis showed the NRs to have an atomic ratio of Pd/Ga = 1.94 (Fig. S1).

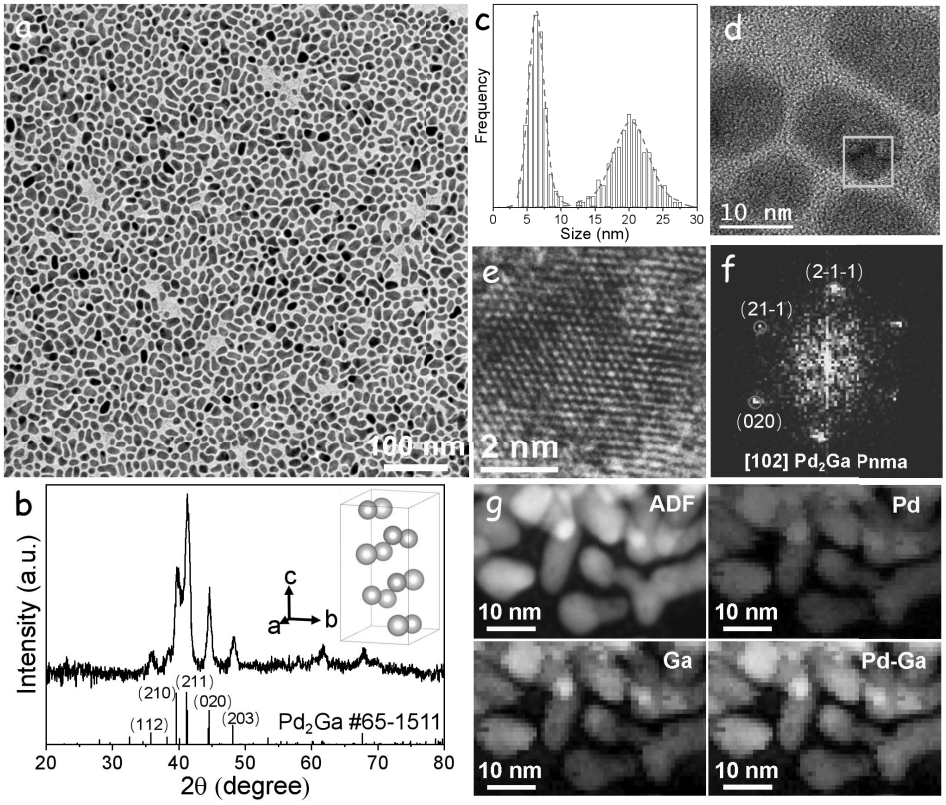

Fig. 1. Structural and chemical characterization of the Pd_2Ga NRs. (a) TEM image. (b) XRD pattern. The inset shows the Pd_2Ga crystal structure. (c) Size distribution histogram. (d-f) HRTEM micrograph (d), magnified detail of the orange square (e), and its corresponding indexed power spectrum observed along the corresponding [102] zone axis of the orthorhombic Pnma Pd_2Ga structure (f). (g) STEM-EELS elemental composition maps.

Fig. 2 shows the Pd 3d and Ga 2p X-ray photoelectron spectroscopy (XPS) spectra of the Pd_2Ga NRs. Two doublets in the Pd 3d spectrum were identified, corresponding to two Pd chemical states. The main Pd component, accounting for 92% of the total Pd detected, was found at a Pd $3d_{5/2}$ binding energy of 335.0 eV, which is associated with a Pd^0 chemical environment.[48] This binding energy was slightly negatively shifted when compared with pure Pd (ca. 335.3 eV), consistently with the presence of a less electronegative element, Ga, modifying the Pd electronic levels. A second doublet, accounting for 8 % of the detected Pd, was located at a higher binding energy of 336.6 eV ($3d_{5/2}$) and 341.8 eV ($3d_{3/2}$). This component was assigned to Pd^{2+} species resulting from the exposure of Pd_2Ga to air, thus undergoing slight surface oxidation. Two doublets were also identified in the Ga 2p XPS spectrum. In this case, the minor one at about 1115.7 eV ($2p_{3/2}$) is associated with Ga^0, and most of the surface Ga is found to be oxidized, in the form of Ga^{3+} at 1118.2 eV ($2p_{3/2}$). The atomic ratio of Pd/Ga obtained by XPS was 0.9. This ratio was significantly lower than the stoichiometric values deduced from XRD, EDS and HRTEM analyses, which points towards a notable Ga enrichment of the Pd_2Ga NRs that may be related to the surface segregation of this element driven by its higher oxygen affinity.[37,47]

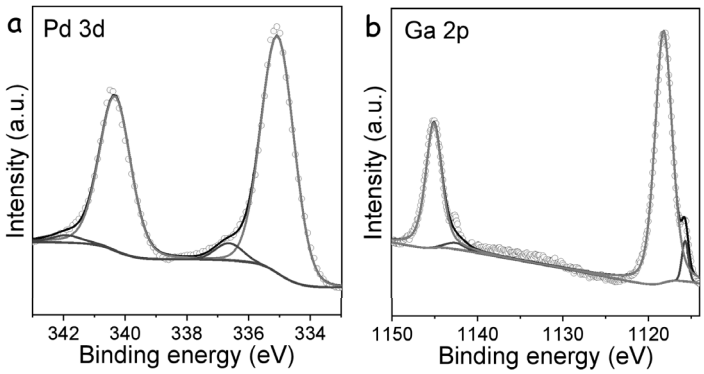

Figure 2. High resolution Pd 3d (a) and Ga 2p (b) XPS spectra of Pd_2Ga.

To investigate the electrocatalytic performance of the as-prepared Pd_2Ga/C electrocatalyst, a three-electrode system using the Pd_2Ga/C catalyst supported on GC as the working electrode was used. Fig. 3a shows the linear sweep voltammetry (LSV) curves measured in 0.5 M KOH aqueous solution with and without 0.5 M ethanol. In the absence of ethanol, a large increase of current density is observed above 1.6 V vs. RHE, which is associated with the oxygen evolution reaction (OER). The potential required to drive the OER at a current density of 10 mA cm^{-2} was 1.69 V vs. RHE. In the presence of ethanol, an abrupt current density increase takes place at a significantly lower potential, about 0.3 V vs. RHE, requiring just 0.51 V to reach a current density of 10 mA cm^{-2}. Thus a 1.18 V lower potential is required to reach similar EOR and OER current densities using the Pd_2Ga/C catalyst.

Fig. 3b displays the CV curves of catalysts obtained in an argon-saturated 0.5 M KOH aqueous solution. The Pd_2Ga/C catalyst displayed similar coulombic features as commercial Pd/C and Pt/C. In the region between 0 V and 0.4 V vs. RHE, hydrogen was adsorbed/desorbed (cathodic/anodic scan) on/from the catalysts surface.[49] The current densities obtained from Pd_2Ga/C and Pt/C catalysts in this region were significantly higher than those of Pd/C, indicating a more effective hydrogen adsorption/desorption processes on their surfaces. As increasing the potential in the anodic scan higher valence oxides are formed on the Pd and Pt surface, which are reduced at around 0.7 V vs. RHE in the cathodic scan. The much more intense reduction peaks obtained from Pd_2Ga/C suggests this catalyst to have a higher electrochemically active surface area than Pd/C and Pt/C.

The EOR electrocatalytic activity of Pd_2Ga/C, Pd/C and Pt/C was investigated in 0.5 M KOH containing 0.5 M ethanol solution. As shown in Fig. 3c, two well-defined peaks associated with the ethanol oxidation in alkaline media were observed for all catalysts, one in the forward and the other in the reverse scan. As observed by LSV, for Pd_2Ga/C, the EOR was activated at ca. 0.3 V vs. RHE in the

forward scan. In contrast, the EOR was activated at ca. 0.4 V vs. RHE in Pd/C and Pt/C catalysts. Besides, the potential required for Pd_2Ga/C to reach a current density of 10 mA cm^{-2} was 0.51 V vs. RHE, which is 0.18 V and 0.09 V lower than that required for Pd/C and Pt/C, respectively. The specific activity, as measured by the peak current density, was up to 164.2 mA cm^{-2} for Pd_2Ga/C, much higher than that of 18.4 mA cm^{-2} for Pd/C and 33.8 mA cm^{-2} for Pt/C. The EOR specific activity of Pd_2Ga/C was significantly above that of state of the art Pd- and Pt-based catalysts (Table S1). Taking into account the noble metal amount in each catalyst, the mass activity calculated for Pd_2Ga/C was 1.97 A mg^{-1}_{Pd}, that is ca. 2.3 and 2.5 times higher than in Pd/C (0.87 A mg^{-1}_{Pd}) and Pt/C (0.80 A mg^{-1}_{Pt}), respectively (Fig. 3d).

During the reverse scan, a current density peak was recorded at ca. 0.7 V vs. RHE, coinciding with the reduction of the Pd/Pt oxides. The ratio of the peak current densities for forward (J_f) and reverse (J_r) scan, J_f/J_r, was 0.91, 1.08 and 1.12, for Pd/C, Pt/C and Pd_2Ga/C, respectively. While some controversy exists on the interpretation of this ratio,[50] the higher J_f/J_r obtained from Pd_2Ga/C is an additional indication of the higher EOR activity of this catalyst.

To evaluate the stability of the catalysts, chronoamperometry (CA) measurements were carried out in a solution containing 0.5 M KOH and 0.5 M ethanol at a potential of ca. 0.8 V versus RHE. As shown in Fig. 4e, the current density of Pd/C and Pt/C decreased dramatically down to a negligible activity during the initial half-hour. Although a strong activity decay was also obtained for Pd_2Ga/C during the first hours of reaction, even after 12h of reaction a significant current density of about 5.2 mA cm^{-2}, was still measured (Fig. S2). This result is especially remarkable taking into account the much higher activity of the Pd_2Ga/C catalysts thus generating a higher amount of intermediates/products that can block active sites. Thus, not mediating any mechanism for the accelerated desorption of these species,

the Pd_2Ga/C catalysts should display a much stronger current density decay than less active Pd/C and Pt/C catalysts.

To gain insight from the current decay, several consecutive CA curves were recorded in periods of 1000 s (Fig. S3). In between these 1000 s periods, 5 CV cycles within the potential range -0.1 V - 1.3 V were conducted to reactivate the catalyst. After each reactivation, the activity of Pd_2Ga/C was fully recovered to the initial current density. This result indicates that the current density decrease was mainly ascribed to the aggregation of reaction intermediates/products on the catalyst surface that blocked the active sites and which could be removed by just rapidly cycling the catalyst in a small potential range.

The product of the electrocatalytic ethanol oxidation remaining in the electrolyte after the CA measurements was analyzed by 1H nuclear magnetic resonance (1H NMR). As shown in Figure 3f, only acetic acid, at a chemical shift of ca. 1.77 ppm, was detected as the oxidation product in the electrolyte. The amount of produced acetic acid for different catalysts was calculated by integrating the peaks at ca. 1.77 ppm. The amount of acetic acid produced by Pd_2Ga/C was 10 times higher than that of Pt/C and 35 times higher than that of Pd/C, which demonstrates the outstanding performance of Pd_2Ga/C for selective conversion of ethanol to acetic acid. In this process, ethanol is initially oxidized to acetaldehyde and this is subsequently oxidized to acetic acid, which is known as the reactive-intermediate pathway.[34,51] Overall, these results demonstrated Pd_2Ga/C to be a highly active, stable and selective catalyst for the electrosynthesis of acetic acid from ethanol.

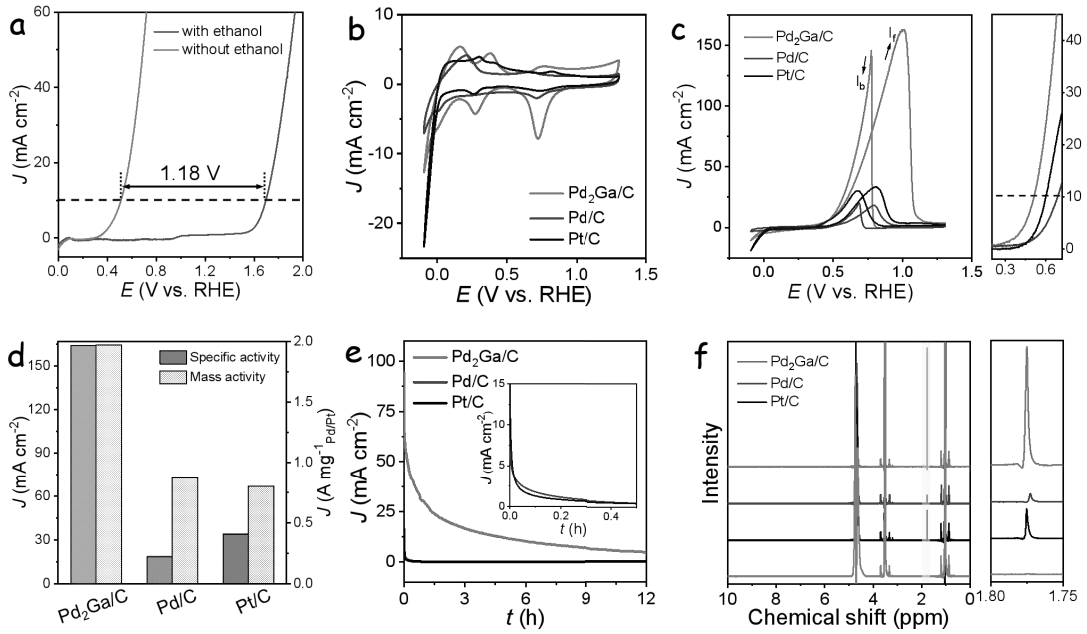

Fig. 3. (a) LSV curves of the Pd_2Ga/C catalyst in 0.5 M KOH with and without 0.5 M ethanol. (b) CV curves of the different catalysts in 0.5 M KOH solution. (c) CV curves of the different catalysts in 0.5 M KOH with 0.5 M ethanol solution. (d) Comparison of the specific and mass activity of the different catalysts. (e) CA measurements in 0.5 M KOH with 0.5 M ethanol solution. (f) 1H NMR analysis of the electrolytes after CA measurements.

The electrocatalytic activity towards HER was also investigated in a 0.5 M KOH containing 0.5 M ethanol electrolyte. Figure 4a displays the LSVs of the different catalysts. To reach a current density of 10 mA cm^{-2}, just 0.13 V was required for Pd_2Ga/C, which was comparable to the voltage required by commercial Pt/C (0.09 V) and much lower than that of the Pd/C catalyst (0.40 V). Furthermore, the Pd_2Ga/C catalyst showed a lower Tafel slope, 174 mV dec^{-1}, than the Pd/C catalyst (452 mV dec^{-1}), indicating a faster HER reaction kinetics on the Pd_2Ga/C surface. Notice also that, while the Tafel slope for the Pt/C catalyst was even lower (100 mV dec^{-1}) as calculated from the small current density range, when increasing the current density towards commercially relevant values, the slope of the LSV

curve increases faster for the Pd_2Ga/C catalyst, to the point that the overpotential to drive 100 mA cm^{-2} is lower for Pd_2Ga/C than for Pt/C.

The durability of the Pd_2Ga catalyst in the HER process was evaluated by chronopotentiometry analysis at two different current densities, 10 mA cm^{-2} and 20 mA cm^{-2}. As shown in Figure 4c, the Pd_2Ga/C catalyst displayed an almost constant potential during the 50 h measurement, confirming its excellent stability under HER conditions. In addition, the faradaic efficiency (FE) of Pd_2Ga/C for hydrogen production measured at different potentials was close to 100% (Fig. 4d). These results demonstrate Pd_2Ga/C to have excellent activity and stability for electrocatalytic hydrogen production in an alkaline electrolyte containing ethanol.

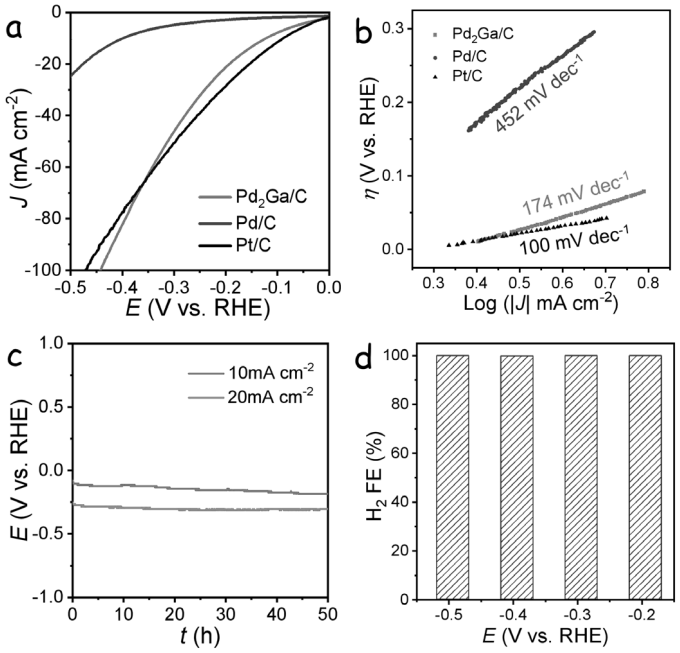

Fig. 4. (a) Polarization curves of catalysts in a solution 0.5 M KOH and ethanol. (b) Tafel plots of the catalysts. (c) Potential-time curves of the Pd_2Ga catalyst at current densities of 10 and 20 mA cm^{-2} in 0.5 M KOH with ethanol solution. (d) FE for the hydrogen production of Pd_2Ga catalyst at different potentials.

Inspired by the excellent electrocatalytic performance of Pd_2Ga/C in both the EOR and HER, a two-electrode electrolyzer was assembled using Pd_2Ga/C as the catalyst for both the anode and cathode in 0.5 M KOH + 0.5 M ethanol electrolyte (Fig. 5a). As a reference, similar electrolyzers using Pd/C or Pt/C as the catalyst in both electrodes were also assembled and measured. Fig. 5b displays the LSV curves of the produced two-electrode systems. To reach a current density of 10 mA cm^{-2}, the system based on the Pd_2Ga/C catalyst required a potential of 0.62 V, much lower than the 0.71 V and 1.11 V required by the Pt/C and Pd/C systems, respectively. Moreover, the Pd_2Ga/C system exhibited a low Tafel slope of 236 mV dec^{-1}, well below that of Pt/C (276 mV dec^{-1}) and Pd/C (597 mV dec^{-1}) (Fig. 5c). These results demonstrated the Pd_2Ga/C to be an excellent bifunctional catalyst for the proposed electrolyzer showing high activity and a favorable charge transfer kinetics.

The durability of the electrolyzer was tested using CA method at a voltage of 0.8 V. As present in Fig. 5d, all catalysts exhibited a pronounced decay in the initial stage, similar to that measured in the three-electrode system for EOR. After 15 h CA measurements, Pd_2Ga was able to maintain a much higher current density than that of Pd/C and Pt/C (Fig. S4). We hypothesize this decay of current density to be related to the adsorption of C2 intermediates in the anodic electrode. This hypothesis was confirmed by the recovery of activity after CV activation after each 1000 s period, as shown in Fig. 5e. Even after the long-term stability measurement, the activity of Pd_2Ga/C catalyst showed little decay after activation compared with the initial activity, further confirming the high stability of Pd_2Ga/C catalyst in the two-electrode coupled system (Fig. 5f).

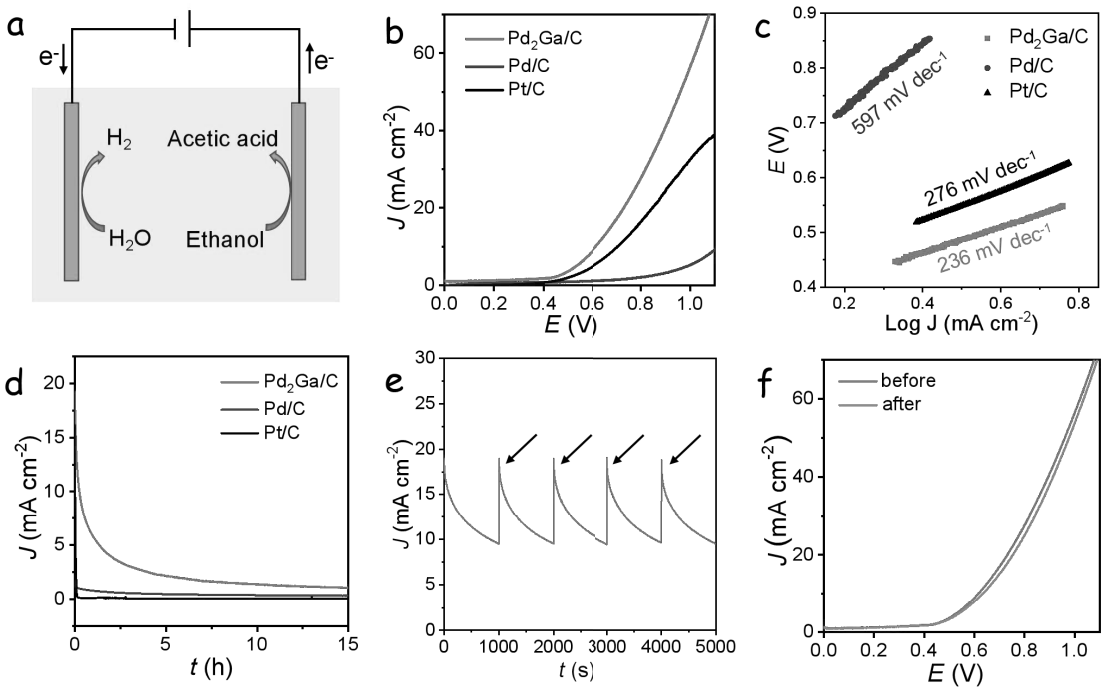

Fig. 5. (a) Schematic diagram of the cell enabling oxidation of ethanol to acetic acid with hydrogen coproduction. (b) LSVs of the cells in 0.5 M KOH with 0.5 M ethanol solution. (c) Tafel plots of the cells based on different catalysts. (d) CA measurements of cells containing 0.5 M KOH with 0.5 M ethanol solution. (e) CA curves of the Pd_2Ga-based cell with CV reactivation every 1000 s. (f) CV curves before and after 15 h CA and reactivation.

To gain insight from the high performance of Pd_2Ga for both HER and EOR, and evaluate the effect of Ga on the Pd_2Ga intermetallic, DFT calculations were conducted on Pd (111) and Pd_2Ga (211) surfaces (Fig. S5). Figure 6a shows the Gibbs free energy of adsorbed H* (ΔG_{H^*}) on Pd (111) and Pd_2Ga (211) active sites. In general, a catalyst with efficient HER performance is expected to have ΔG_{H^*} close to zero, providing both a fast release of hydrogen and proton/electron-transfer process. Based on the calculation results, Pd_2Ga presented a lower $|\Delta G_{H^*}|$ than Pd, which is consistent with the higher HER activity measured on Pd_2Ga compared with Pd.

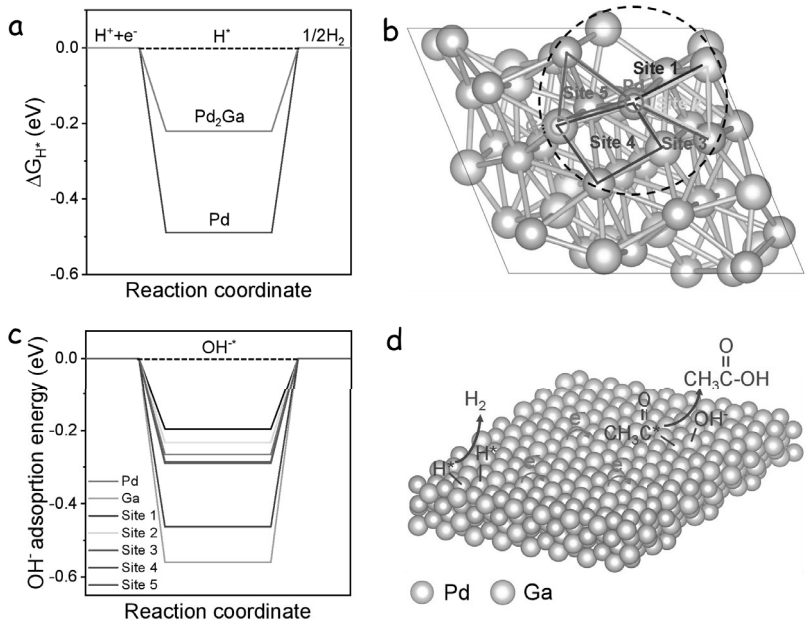

Fig. 6. (a) Free-energy diagram for atomic hydrogen adsorption on the Pd and Pd_2Ga surface. (b) Absorption sites on the Pd_2Ga surface. (c) The adsorption energy of OH^- on different adsorption sites of Pd_2Ga surface. (d) The scheme of the electronic effect and synergetic catalytic effect for enhanced HER and EOR on Pd_2Ga/C catalyst.

The EOR performance is related to the adsorption/desorption energy of reaction intermediates on the surface of the catalyst. For the reactive-intermediate EOR pathway on Pd-based catalysts, the stripping of acetic acid from the surface of the catalyst is very fast, and the reaction of absorbed acetyl with hydroxyl to produce acetic acid is generally regarded as the rate-limiting step.[12,16] A high adsorption ability of OH^- usually facilitates the formation of acetic acid and thus increases the EOR activity. Thus, the adsorption energy of OH^- at Pd and Ga sites, as well as the different adsorption sites around the Pd site at Pd_2Ga surface were calculated (Fig. 6b). As presented in Fig. 6c and Fig. S6, the lowest adsorption energies corresponded to the adsorption of OH^- on the top of Ga site. The high binding energy of OH^- on Ga site is associated with the electronegativity difference between Pd and

Ga, which results in a shift of the electron cloud towards the Pd. Thus, the positively charged Ga is a very effective OH^- adsorption site. This high adsorption ability of OH^- on Ga sites not only facilitates overcoming the EOR barriers of the rate-limiting step, but also helps to free the Pd active sites for the ethanol adsorption and their further oxidation, thus enhancing not only the EOR activity but also its durability (Fig. 6d).

4. Conclusions

In summary, a novel colloidal method was developed to produce monodispersed Pd_2Ga nanorods with an average size of 7×20 nm. As an electrocatalyst for EOR, Pd_2Ga/C delivers a peak current density of 164.2 mA cm^{-2} and a mass activity of 1.97 A mg^{-1}_{Pd}. Moreover, the Pd_2Ga/C catalyst exhibits a high selectivity towards acetic acid in the EOR process. Pd_2Ga also display excellent performance as HER catalyst in a KOH electrolyte containing ethanol, with a very low overpotential of 0.13 V and close 100% FE for hydrogen production. A two-electrode electrolyzer using Pd_2Ga/C as bifunctional electrocatalyst for both the anodic EOR and cathodic HER required just 0.62 V to run the H_2 and acetic acid production at a current density of 10 mA cm^{-2}. DFT calculations revealed that the presence of Ga could tune the electronic structure of Pd, leading to weakened hydrogen-binding energy on Pd sites. Besides, Ga sites allowed an enhanced binding ability of OH^-, which explains the fast kinetics and activity of Pd_2Ga. This work provides a novel catalyst and a promising method for the simultaneous production of acetic acid and hydrogen fuel at low voltage and high efficiency, as an example of a promising strategy for the production of value-added fine chemicals coupled with hydrogen generation.

Declaration of competing interest

The authors declare that they have no known competing financial interests or personal relationships that could have appeared to influence the work reported in this paper.

Acknowledgements

This work was supported by the National Natural Science Foundation of China (No. 22008091), the funding for scientific research startup of Jiangsu University (No. 19JDG044), and Jiangsu Provincial Program for High-Level Innovative and Entrepreneurial Talents Introduction. ICN2 acknowledges funding from Generalitat de Catalunya 2017 SGR 327. The authors thank support from the project NANOGEN (PID2020-116093RB-C43), funded by MCIN/ AEI/10.13039/501100011033/. ICN2 is supported by the Severo Ochoa program from Spanish MINECO (Grant No. SEV-2017-0706) and is funded by the CERCA Programme / Generalitat de Catalunya.

References

[1] F. A. Garcés-Pineda, M. Blasco-Ahicart, D. Nieto-Castro, N. López, J. R. Galán-Mascarós, Direct magnetic enhancement of electrocatalytic water oxidation in alkaline media, Nat. Energy 4 (2019) 519-525.

[2] P. Zhai, M. Xia, Y. Wu, G. Zhang, J. Gao, B. Zhang, S. Cao, Y. Zhang, Z. Li, Z. Fan, C. Wang, X. Zhang, J. T. Miller, L. Sun, J. Hou, Engineering single-atomic ruthenium catalytic sites on defective nickel-iron layered double hydroxide for overall water splitting, Nat. Commun. 12 (2021) 4587.

[3] B. You, M. T. Tang, C. Tsai, F. Abild-Pedersen, X. Zheng, H. Li, Enhancing Electrocatalytic Water Splitting by Strain Engineering, Adv. Mater. 31 (2019) 1807001.

[4] H. Zhang, W. Cheng, D. Luan, X. W. Lou, Atomically Dispersed Reactive Centers for

Electrocatalytic CO_2 Reduction and Water Splitting, Angew. Chem. Int. Ed. 60 (2020) 13177-13196.

[5] Z. Zhang, X. Wu, Z. Kou, N. Song, G. Nie, C. Wang, F. Verpoort, S. Mu, Rational design of electrospun nanofiber-typed electrocatalysts for water splitting: A review, Chem. Eng. J. 428 (2022) 131133.

[6] J. Zhang, S. Guo, B. Xiao, Z. Lin, L. Yan, D. Du, S. Shen, Ni-Mo based mixed-phase polyionic compounds nanorod arrays on nickel foam as advanced bifunctional electrocatalysts for water splitting, Chem. Eng. J. 416 (2021) 129127.

[7] Y. Zhang, B. Zhou, Z. Wei, W. Zhou, D. Wang, J. Tian, T. Wang, S. Zhao, J. Liu, L. Tao, S. Wang, Coupling Glucose-Assisted Cu(I)/Cu(II) Redox with Electrochemical Hydrogen Production, Adv. Mater. 33 (2021) 2104791.

[8] J. Zhang, T. He, M. Wang, R. Qi, Y. Yan, Z. Dong, H. Liu, H. Wang, B. Y. Xia, Energy-saving hydrogen production coupling urea oxidation over a bifunctional nickel-molybdenum nanotube array, Nano Energy 60 (2019) 894-902.

[9] S. L. Fereja, P. Li, Z. Zhang, J. Guo, Z. Fang, Z. Li, S. He, W. Chen, W-doping induced abundant active sites in a 3D NiS_2/MoO_2 heterostructure as an efficient electrocatalyst for urea oxidation and hydrogen evolution reaction, Chem. Eng. J. 432 (2022) 134274.

[10] T. Wang, L. Tao, X. Zhu, C. Chen, W. Chen, S. Du, Y. Zhou, B. Zhou, D. Wang, C. Xie, P. Long, W. Li, W. Wang, R. Chen, Y. Zou, X. Fu, Y. Li, X. Duan, S. Wang, Combined anodic and cathodic hydrogen production from aldehyde oxidation and hydrogen evolution reaction, Nat. Catal. 5 (2022) 66-73.

[11] K. Yin, Y. Chao, F. Lv, L. Tao, W. Zhang, S. Lu, M. Li, Q. Zhang, L. Gu, H. Li, S. Guo, One Nanometer PtIr Nanowires as High-Efficiency Bifunctional Catalysts for Electrosynthesis of Ethanol into High Value-Added Multicarbon Compound Coupled with Hydrogen Production, J. Am. Chem. Soc. 143 (2021) 10822-10827.

[12] D. Si, B. Xiong, L. Chen, J. Shi, Highly selective and efficient electrocatalytic synthesis of glycolic acid in coupling with hydrogen evolution, Chem Catal. 1 (2021) 941-955.

[13] C. Wang, H. Lu, Z. Mao, C. Yan, G. Shen, X. Wang, Bimetal Schottky Heterojunction Boosting Energy-Saving Hydrogen Production from Alkaline Water via Urea Electrocatalysis, Adv. Funct. Mater. 30 (2020) 2000556.

[14] M. Wu, J. Zhao, C. Li, R. Liu, Heterogeneity in a metal–organic framework in situ guides engineering Co@CoO heterojunction for electrocatalytic H_2 production in tandem with glucose oxidation, J. Mater. Chem. A 10 (2022) 4791-4799.

[15] Y. Xu, B. Zhang, Recent Advances in Electrochemical Hydrogen Production from Water Assisted by Alternative Oxidation Reactions, ChemElectroChem 6 (2019) 3214-3226.

[16] X. Yu, J. Liu, J. Li, Z. Luo, Y. Zuo, C. Xing, J. Llirca, D. Nasiou, J. Arbiol, K. Pan, T. Kleinhanns, Y. Xie, A. Cabot, Phosphorous incorporation in Pd_2Sn alloys for electrocatalytic ethanol oxidation, Nano Energy 77 (2020) 105116.

[17] M. Zhou, J. Liu, C. Ling, Y. Ge, B. Chen, C. Tan, Z. Fan, J. Huang, J. Chen, Z. Liu, Z. Huang, J. Ge, H. Cheng, Y. Chen, L. Dai, P. Yin, X. Zhang, Q. Yun, J. Wang, H. Zhang, Synthesis of Pd_3Sn and PdCuSn Nanorods with $L1_2$ Phase for Highly Efficient Electrocatalytic Ethanol Oxidation, Adv. Mater. 34 (2022) 2106115.

[18] H. Xiao, S. Xue, J. Zhang, M. Zhao, J. Ma, S. Chen, Z. Zheng, J. Jia, H. Wu, Facile electrolytic synthesis of Pt and carbon quantum dots coloaded multiwall carbon nanotube as highly efficient electrocatalyst for hydrogen evolution and ethanol oxidation, Chem. Eng. J. 408 (2021) 127271.

[19] G. Chen, Y. Luo, L. Ding, H. Wang, Low-Voltage Electrolytic Hydrogen Production Derived from Efficient Water and Ethanol Oxidation on Fluorine-Modified FeOOH Anode, ACS Catal. 8 (2018) 526-530.

[20] K. M. Lee, J. H. Jang, M. Balamurugan, J. E. Kim, Y. I. Jo, K. T. Nam, Redox-neutral electrochemical conversion of CO_2 to dimethyl carbonate, Nat. Energy, 6 (2021) 733-741.

[21] Y. Qin, H. Huang, W. Yu, H. Zhang, Z. Li, Z. Wang, J. Lai, L. Wang, S. Feng, Porous PdWM (M = Nb, Mo and Ta) Trimetallene for High C1 Selectivity in Alkaline Ethanol Oxidation Reaction, Adv. Sci. 9 (2021) 2103722.

[22] S. He, Y. Liu, H. Li, Q. Wu, D. Ma, D. Gao, J. Bi, Y. Yang, C. Cui, Highly Dispersed Mo Sites on

Pd Nanosheets Enable Selective Ethanol-to-Acetate Conversion, ACS Appl. Mater. Interf. 13 (2021) 13311-13318.

[23] Q. He, D. Tian, H. Jiang, D. Cao, S. Wei, D. Liu, P. Song, Y. Lin, L. Song, Achieving Efficient Alkaline Hydrogen Evolution Reaction over a Ni_5P_4 Catalyst Incorporating Single-Atomic Ru Sites, Adv. Mater. 32 (2020) 1906972.

[24] X. F. Lu, L. Yu, J. Zhang, X. W. Lou, Ultrafine Dual-Phased Carbide Nanocrystals Confined in Porous Nitrogen-Doped Carbon Dodecahedrons for Efficient Hydrogen Evolution Reaction, Adv. Mater., 31 (2019) 1900699.

[25] J. Kim, H. Jung, S. Jung, J. Hwang, D. Y. Kim, N. Lee, K. Kim, H. Kwon, Y. Kim, J. W. Han, J. K. Kim, Tailoring Binding Abilities by Incorporating Oxophilic Transition Metals on 3D Nanostructured Ni Arrays for Accelerated Alkaline Hydrogen Evolution Reaction, J. Am. Chem. Soc. 143 (2021) 1399-1408.

[26] W. Du, Y. Shi, W. Zhou, Y. Yu, B. Zhang, Unveiling the In Situ Dissolution and Polymerization of Mo in Ni_4Mo Alloy for Promoting the Hydrogen Evolution Reaction, Anew. Chem. Int. Ed. 60 (2021) 7051-7055.

[27] H. Song, Y. Li, L. Shang, Z. Tang, T. Zhang, S. Lu, Designed controllable nitrogen-doped carbon-dots-loaded MoP nanoparticles for boosting hydrogen evolution reaction in alkaline medium, Nano Energy, 2020, 72, 104730.

[28] F. Yu, Z. Lang, L. Yin, K. Feng, Y. Xia, H. Tan, H. Zhu, J. Zhong, Z. Kang, Y. Li, Pt-O bond as an active site superior to Pt0 in hydrogen evolution reaction, Nat. Common. 11 (2020) 490.

[29] S. Fang, X. Zhu, X. Liu, J. Gu, W. Liu, D. Wang, W. Zhang, Y. Lin, J. Lu, S. Wei, Y. Li, T. Yao, Uncovering near-free platinum single-atom dynamics during electrochemical hydrogen evolution reaction, Nat. Common. 11 (2020) 1029.

[30] S. Sarkar, S. C.. Peter, An overview on Pd-based electrocatalysts for the hydrogen evolution reaction, Inorg. Chem. Front. 5 (2018) 2060-2080.

[31] Z. Wang, B. Xiao, Z. Lin, Y. Xu, Y. Lin, F. Meng, Q. Zhang, L. Gu, B. Fang, S. Guo, W. Zhong, $PtSe_2$/Pt Heterointerface with Reduced Coordination for Boosted Hydrogen Evolution Reaction,

Anew. Chem. Int. Ed. 133 (2021) 23576-23581.

[32] S. Huang, S. Lu, H. Hu, F. Xu, H. Li, F. Duan, H. Zhu, H. Gu, M. Du, Hyper-dendritic PdZn nanocrystals as highly stable and efficient bifunctional electrocatalysts towards oxygen reduction and ethanol oxidation, Chem. Eng. J. 420 (2021) 130503.

[33] S. Luo, L. Zhang, Y. Liao, L. Li, Q. Yang, X. Wu, X. Wu, D. He, C. He, W. Chen, Q. Wu, M. Li, E. J. M. Hensen, Z. Quan, A Tensile-Strained Pt-Rh Single-Atom Alloy Remarkably Boosts Ethanol Oxidation, Adv. Mater. 33 (2021) 2008508.

[34] Y. Qiu, J. Zhang, J. Jin, J. Sun, H. Tang, Q. Chen, Z. Zhang, W. Sun, G. Meng, Q. Xu, Y. Zhu, A. Han, L. Gu, D. Wang, Y. Li, Construction of Pd-Zn dual sites to enhance the performance for ethanol electro-oxidation reaction, Nat. Common. 12 (2021) 5273.

[35] H. Wang, L. Jiao, L. Zheng, Q. Fang, Y. Qin, X. Luo, X. Wei, L. Hu, W. Gu, J. Wen, C. Zhu, PdBi Single-Atom Alloy Aerogels for Efficient Ethanol Oxidation, Adv. Funct. Mater. 31 (2021) 2103465.

[36] X. Zhou, Y. Ma, Y. Ge, S. Zhu, Y. Cui, B. Chen, L. Liao, Q. Yun, Z. He, H. Long, L. Li, B. Huang, Q. Luo, L. Zhai, X. Wang, L. Bai, G. Wang, Z. Guan, Y. Chen, C. Lee, J. Wang, C. Ling, M. Shao, Z. Fan, H. Zhang, Preparation of Au@Pd Core−Shell Nanorods with fcc-2H-fcc Heterophase for Highly Efficient Electrocatalytic Alcohol Oxidation, J. Am. Chem. Soc. 144 (2021) 547-555.

[37] X. Yu, Z. Luo, T. Zhang, P. Tang, J. Li, X. Wang, J. Llorca, J. Arbiol, J. Liu, A. Cabot, Stability of Pd_3Pb Nanocubes during Electrocatalytic Ethanol Oxidation, Chem. Mater. 32 (2020) 2044-2052.

[38] A. L. Allred, Electronegativity values from thermochemical data, J. Inorg. Nuclear Chem. 17 (1961) 215-221.

[39] G. Kresse, J. Hafner, Ab initio molecular dynamics for liquid metals, Phys. Rev. B 47 (1993) 558-.

[40] G. Kresse, J. Furthmüller, Efficiency of ab-initio total energy calculations for metals and semiconductors using a plane-wave basis set, Comp Mater Sci. 6 (1996) 15-50.

[41] J. P. Perdew, Y. Wang, Accurate and simple analytic representation of the electron-gas correlation energy, Phys Rev B 45 (1992) 13244.

[42] J. P. Perdew, K. Burke, M. Ernzerhof, Generalized Gradient Approximation Made Simple, Phys. Rev. Lett. 77 (1996) 3865.

[43] P. E. Blöchl, Projector augmented-wave method, Phys. Rev. B 50 (1994) 17953.

[44] S. Grimme, J. Antony, S. Ehrlich, H. Krieg, A consistent and accurate ab initio parametrization of density functional dispersion correction (DFT-D) for the 94 elements H-Pu, J. Chem. Phys. 132 (2010) 154104.

[45] S. Grimme, S. Ehrlich, L. Goerigk, Effect of the damping function in dispersion corrected density functional theory, J. Comput. Chem. 32 (2011) 1456-1465.

[46] J. Liu, Z. Luo, J. Li, X. Yu, J. Llorca, D. Nasiou, J. Arbiol, M. Meyns, A. Cabot, Graphene-supported palladium phosphide PdP_2 nanocrystals for ethanol electrooxidation, Appl. Catal. B Environ. 242 (2019) 258-266.

[47] Z. Luo, J. Lu, C. Flox, R. Nafria, A. Genç, J. Arbiol, J. Llorca, M. Ibáñez, J. R. Morante, A. Cabot, Pd_2Sn [010] Nanorods as a Highly Active and Stable Ethanol Oxidation Catalyst, J. Mater. Chem. A, 4 (2016) 16706-16713.

[48] J. F. Moulder, W. F. Stickle, P. E. Sobol, K. D. Bomben, Handbook of X-ray Photoelectron Spectroscopy: A Reference Book of Standard Spectra for Identification and Interpretation of XPS Data, PerkinElmer, Physical Electronics Division: Eden Prairie, MN 1992.

[49] Z. X. Liang, T. S. Zhao, J. B. Xu, L. D. Zhu, Mechanism study of the ethanol oxidation reaction on palladium in alkaline media, Electrochim. Acta 54 (2009) 2203-2208.

[50] Y. Zhao, X. Li, J. M. Schechter, Y. Yang, Revisiting the oxidation peak in the cathodic scan of the cyclic voltammogram of alcohol oxidation on noble metal electrodes, RSC Adv. 6 (2016) 5384-5390.

[51] D. Wu, K. Kusada, T. Yamamoto, T. Toriyama, S. Matsumura, S. Kawaguchi, Y. Kubota, H. Kitagawa, Platinum-group-metal high-entropy-alloy nanoparticles, J. Am. Chem. Soc. 142 (2020) 13833-13838.

Declaration of interests

☒The authors declare that they have no known competing financial interests or personal relationships that could have appeared to influence the work reported in this paper.

☐The authors declare the following financial interests/personal relationships which may be considered as potential competing interests: